

Estimation of Ground Strain Using Accelerograms Recorded by Two Dense Seismic Arrays at Lotung, Taiwan

Jen-Kuang Chung^{1, *}

(Manuscript received 28 December 2006, in final form 23 April 2007)

ABSTRACT

In this study, ground strains over a soft sediment-filled plain were estimated for nineteen moderate earthquakes in northeastern Taiwan. To this end, abundant accelerograms recorded by two independent seismic arrays, LLSST and SMART1, were analyzed. These two dense seismic arrays are both highly overlapping in terms of space and operation duration. Spatial analyses herein for the LLSST array suggest that good estimates of ground strains can be obtained using only three 3-component seismometers recording at stations configured in a simple triangle with maximum separation of about 100 m.

In the case of the Hualien earthquake ($M_L = 6.5$) of 20 May 1986, a peak shear strain of 210μ occurs with direct S-waves whilst strain of 186μ occurs with surface waves dominated by a period of about 2.5 sec. However, the peak vertical gradient accompanied by shear waves is in the range $1500 \sim 2000\mu$, which is larger than that of horizontal differential motion by a factor of about 10.

For further applications in mapping ground deformation fields at a given region, the single-station method is examined by comparing its estimates with those of a displacement gradient algorithm. A moving cross-correlation method is proposed to obtain phase velocities for a sequence of waves, particularly when ground motion contains obvious surface-wave energy. Consequently, estimates of peak horizontal strain at the LLSST site are in the range $1 \sim 150\mu$ for the nineteen moderate earthquakes and the logarithm of these appears to be proportional to earthquake magnitudes.

¹ General Education Center, Ching Yun University of Technology, Chung-Li, Taiwan, ROC

* *Corresponding author address:* Prof. Jen-Kuang Chung, General Education Center, Ching Yun University of Technology, Chung-Li, Taiwan, ROC; E-mail: jkchung@cyu.edu.tw

doi: 10.3319/TAO.2007.18.4.715(T)

Finally, a simple test was implemented to verify the feasibility of this method when used with large station spacing (2 ~ 3 km), simulated by the SMART1 array. In general, when taking strain estimated from LLSST data as a basis, the results from SMART1 reveal that differences would not be over 50%.

(Key words: Ground strain, Differential motion, LLSST array)

1. INTRODUCTION

After the devastation brought by the Michoacan earthquake of 19 September 1985 to Mexico City, the basin in which it was set has become a target for investigating ground behavior associated with nearby or distant great earthquakes (Anderson et al. 1986). From a seismic disaster mitigation viewpoint, the seismic safety of buried lifelines (water lines, oil and gas lines, and tunnels) and long-span structures (bridges, railways, and overpasses) is identified as an important consideration in metropolitan areas subject to such events. Damage occurring in the Bay Area of San Francisco, California during the Loma Prieta earthquake of 18 October 1989 ($M = 7.0$) underscores this importance. Reports from Loma Prieta show most of the liquefaction and damage to pipelines, building foundations, streets, and curbs occurred in areas of artificial fill consisting mainly of loose sand. One factor of concern was peak ground velocities of 30 to 50 cm sec⁻¹ recorded in the Oakland area, while, differential extensional displacements, in the order of 10 cm, were deduced by comparing double integrations of accelerograms recorded on both sides of the East Bay Crossing (Bonilla 1991; Hanks and Brady 1991). In many regions of the world covered by poorly consolidated sediments, most earthquake damage is caused by high peak ground motions. However, the variability of ground motion depends on amplification effects (these include wave focusing and enhanced duration), particularly within three-dimensional basin structures filled with alluvium (Bard and Bouchon 1985; Frankel 1994; Teng and Qu 1996). In this situation, strong motion is generally induced by the superposition of waves coming from multiple directions. Corresponding differential motion or strain could be magnified at certain sites where large-amplitude waves arrive with a phase shift. To support this standpoint, Moczo et al. (1996) have shown by numerical computations that significant spectral amplification and differential motion can arise in a simple trough at the bottom of a horizontal surface sedimentary layer.

Dynamic strain caused by the passage of seismic waves, as distinct from static strain accompanied by permanent distortion, can be estimated using the differentials between any two seismograms recorded at adjacent sites (Saito 1968; Bouchon 1980). In order to obtain scaling relationships for peak strain, forward calculations from synthetic seismograms are performed for a wide range of magnitudes, source to station distances, local soil conditions, and focal mechanisms (Bouchon and Aki 1982; Lee 1990; Trifunac and Lee 1996). However, application of numerical simulations is typically restricted to simple models. This results in difficulty in modeling ground motion due to lateral heterogeneities in regions of interest. Owing to limitations in theoretical modeling, endeavors have been made to obtain more reliable estimations of differential ground motion at given sites utilizing, where possible, surface and/or

borehole seismic recordings from the earthquakes of interest (Smith et al. 1982; Gomberg and Bodin 1994; Spudich et al. 1995; Bodin et al. 1997; Singh et al. 1997). Most of these studies used seismic data from a few distant earthquakes collected by sparse microarrays with station spacings of hundreds of meters. These data are suitable for estimating strains mostly attributable to surface waves. However, due to the plane-wave approximation, the level of estimated strains, in some worst cases, was nearly twice that measured from strainmeters (Gomberg and Agnew 1996). In this article, a large number of accelerograms from one dense three-dimensional seismic array (37 stations), located in northeastern Taiwan, are analyzed to estimate dynamic strains produced by tens of moderate earthquakes ($3.7 \leq M \leq 6.8$) at source distances of 10 to 150 km. The expected advantage is procured by the smallest station spacing being only about 10 m, providing the ability to increase frequency resolution in the range of interest to engineering; i.e., up to ~ 3 Hz. This frequency range is generally associated with strong shear waves and short-period surface waves.

It can be shown that peak ground shear strain is proportional to the maximum velocity of ground motion, but the scaling factor (phase velocity of a seismic wave) is suggested to be dependent on the wave type, component of strain tensor, near-surface structure, and approximations relevant to elastic wave theory. Such a simple relation implies seismic hazard microzonation has a lot of potential, if ground motion recordings from arrays of densely deployed stations are available, and phase velocity at each site can be properly estimated.

Hence, this paper aims at proposing a method for estimating phase velocities relevant to peak ground strains from recordings at adjacent stations. Using this method, the results here could be used to evaluate the feasibility of mapping peak ground strain distribution for some metropolitan areas in Taiwan, where strong-motion observatory networks have operated for a decade, albeit without differential ground motions derived from functional dense arrays and a lack of direct measurements from strainmeters.

2. SEISMIC ARRAYS

Abundant accelerograms recorded by two independent seismic arrays at the same location were analyzed to obtain ground strains from seismic records. The first array, called the Lotung Large Scale Seismic Test (LLSST), was installed and operated from 1985 to 1991 by the Institute of Earth Sciences, Academia Sinica (IESAS), Taiwan, under a joint project with the Taipower Company and the U.S. Electric Power Research Institute. The LLSST microarray was located to the south of the Lanyang plain of northeastern Taiwan (Fig. 1): this is an area very close to station O08 of another large-aperture array named SMART1 at Lotung City. This LLSST microarray was a dense array of thirty-seven stations, arranged in three-dimensional configuration, i.e., fifteen free-surface stations, eight downhole stations (Fig. 2), and fourteen stations in the concrete containment structure. Spacing between the free-surface stations was from 3 to 90 m; and depths for each set of downhole arrays were 6, 11, 17, and 47 m, respectively. Each station was instrumented with a three-component force-balance accelerometer (FBA-13 or FBA-13DH for downhole sites) and a DSA-3 digital recorder for data acquisition.

The SMART1 (Strong Motion ARray in Taiwan #1) array, conducted by the IESAS and the University of California at Berkeley in 1980, consisted of forty-one stations including a

central station and four outer ones, extending in a NS direction approximately. The others were configured in three concentric rings, each having twelve instruments, with radii of 200 m, 1 km, and 2 km, respectively (Fig. 1) (Bolt et al. 1982). These dimensions and configuration minimized spatial aliasing of strong ground motions with frequencies in the range 0.5 to 5 Hz. Each station was equipped with a triaxial force-balance accelerometer (SA-3000) and a DR-100 digital recorder of sampling rate 100 sps, different from the 200 sps of LLSST stations. This array was phased out in 1991 after collecting 978 records from sixty earthquakes.

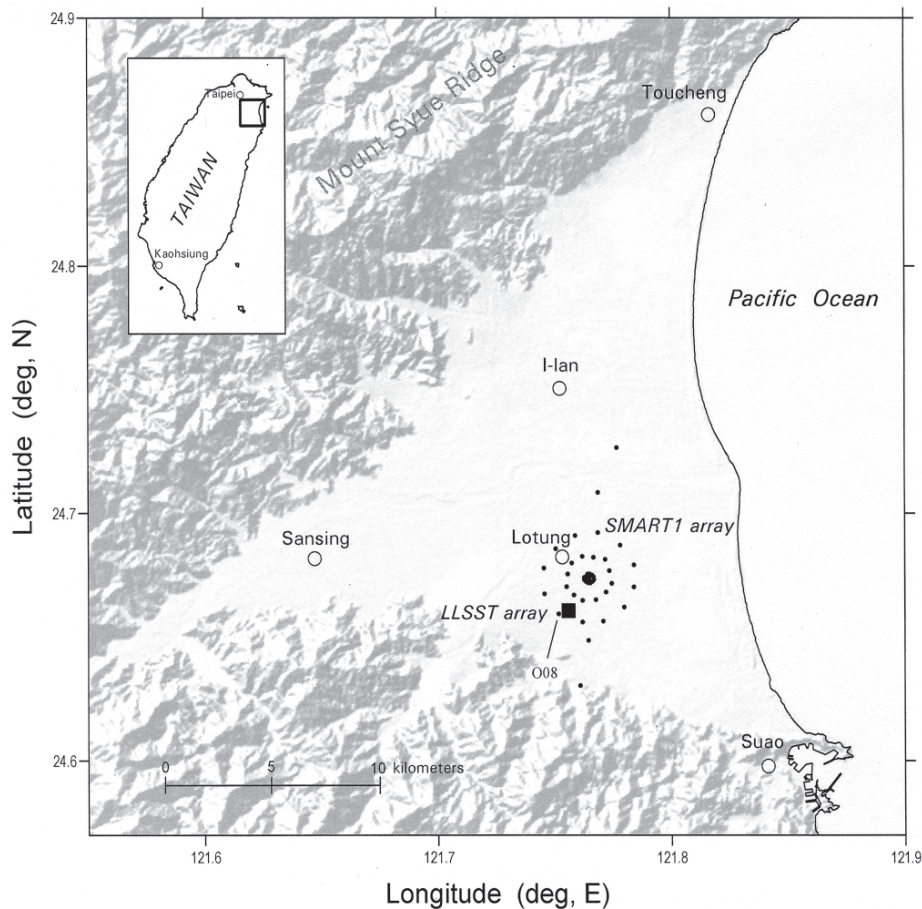


Fig. 1. Locations of the LLSST array (solid square) and SMART1 array (small dots) in the Lanyang plain, Ilan County, Taiwan. The plain is surrounded by the Mount Syue Ridge and the Central Ridge, respectively, on the western and southern sides. The configuration of the LLSST array is sketched in Fig. 2. One of the outer-ring stations of the SMART1 array, O08, is only 300 m away from LLSST.

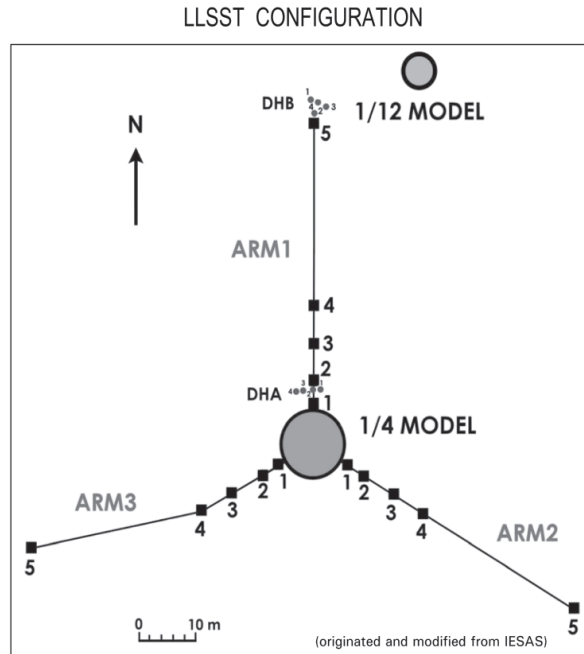


Fig. 2. The surface configuration of the LLSST seismic array at Lotung, Taiwan. The depths for borehole stations of arrays, DHA and DHB, are 6, 11, 17, and 47 m, respectively. The structural stations in the containment models are not shown.

3. GEOLOGIC SETTING

The Lanyang (Ilan) plain in northeastern Taiwan is along the extension of the Okinawa trough, which is considered to be a tensional feature. It is a very flat delta-like alluvial plain of about 300 km². According to seismic surveying and drilling (Chiang 1976), the Lanyang plain is underlain by two layers of recent alluvium (including the soil layer) and a Pleistocene stratum over a Miocene basement. The basement surface is concave upward and inclines eastwards reaching a maximum depth of 1500 m at the central section of the coastline. A well-schemed seismic refraction survey was performed in the SMART1 array area (Wen and Yeh 1984) to aid interpretation of strong-motion recordings. Their results show that the top soil layer from 3 to 18 m and the alluvium layer from 30 to 60 m have P-wave velocities of 430 ~ 760 m sec⁻¹ and 1400 ~ 1700 m sec⁻¹, respectively. A more detailed report, concluded from geotechnical investigation at the Lotung site (LLSST array), shows that from the surface to a depth of 4 meters, the soil is a layer of grey silty sands with a little gravel of about 0.5 to 2 cm in size (Wu et al. 1987). From a depth of about 4 m down to 37 m, in general, the soil layer consists of alternating and interbedded layers of silty sands, clayey silts, and sandy silts with gravel or clay.

4. DATA

Earthquake events were selected based on at least ten of the free-field stations of the LLSST array being triggered to record uncontaminated ground motion. As a consequence, nineteen earthquakes within an epicentral-distance range of 5 to 88 km qualified for estimating ground strains. Source parameters are given in Table 1 and the locations of these earthquakes shown in Fig. 3. Note that peak ground acceleration recorded at the free-field sensors of the

Table 1. Source parameters of earthquakes.

No ¹	Origin Time (UT)		Epicenter		Focal Depth (km)	Epicentral Distance (km)	ML	PGA (gal)	No ²
			Lat.(°N)	Long.(°E)					
4	1986/01/16	13:04	24.763	121.961	10.2	24	6.1	278	39
5	1986/03/29	07:17	24.603	121.810	10.3	8	3.9	60	
6	1986/04/08	02:14	24.379	121.786	10.9	31	4.9	43	
7	1986/05/20	05:25	24.082	121.591	15.8	66	6.1	289	40
8	1986/05/20	05:37	24.048	121.617	21.8	69	5.8	43	41
9	1986/07/11	18:25	24.622	121.783	1.1	9	3.7	169	
10	1986/07/16	23:50	24.608	121.772	1.0	6	3.7	100	
11	1986/07/17	00:03	24.660	121.815	2.0	6	4.3	157	
12	1986/07/30	11:31	24.629	121.794	1.5	5	5.8	254	43
14	1986/07/30	11:38	24.640	121.796	2.3	5	4.2	82	
16	1986/11/14	21:20	23.992	121.833	15.0	74	6.8	167	45
17	1986/11/14	23:04	23.866	121.711	33.0	88	6.3	41	
19	1986/12/08	09:38	24.305	121.966	26.7	45	5.3	63	
21	1987/01/06	05:07	23.914	121.840	28.6	83	5.7	38	
24	1987/06/27	07:38	24.323	121.631	0.5	39	5.1	30	53
25	1987/11/10	04:33	24.418	121.724	34.4	27	4.9	145	54
28	1990/01/15	12:42	24.360	121.932	20.1	38	5.2	94	
29	1990/04/15	22:44	24.357	121.990	22.1	41	4.6	60	
30	1990/07/16	19:14	24.184	121.804	1.4	53	5.1	19	

§ No¹ : No. in catalog of the LLSST array

§ No² : No. in catalog of the SMART1 array

§ PGA : Peak ground acceleration recorded at surface stations of the LLSST array

array may range from 0.1 to 0.3 g for some events. Figure 4 represents some accelerograms in common timing, which were synchronized using an omega clock of accuracy ± 0.0005 sec when collecting data from the seismometers. In terms of data assessment, procedures for doing baseline corrections for seismograms have been proven by testing several artificial extreme cases with major offsets or linear trends. Synchronized acceleration recordings were demeaned and then double-integrated in the frequency domain to obtain displacement. Corrections associated with instrument effects were omitted because response is almost flat with a value of one in a wide frequency range during the period of interest. However, assuming a shear velocity of about 200 m s^{-1} in the soil, for depressing long-period integration noise, a sixth-order zero-phase Butterworth filter with a frequency band from 0.3 to 3 Hz was tapered on the displacement spectrum to avoid spatial aliasing from signals of higher frequencies.

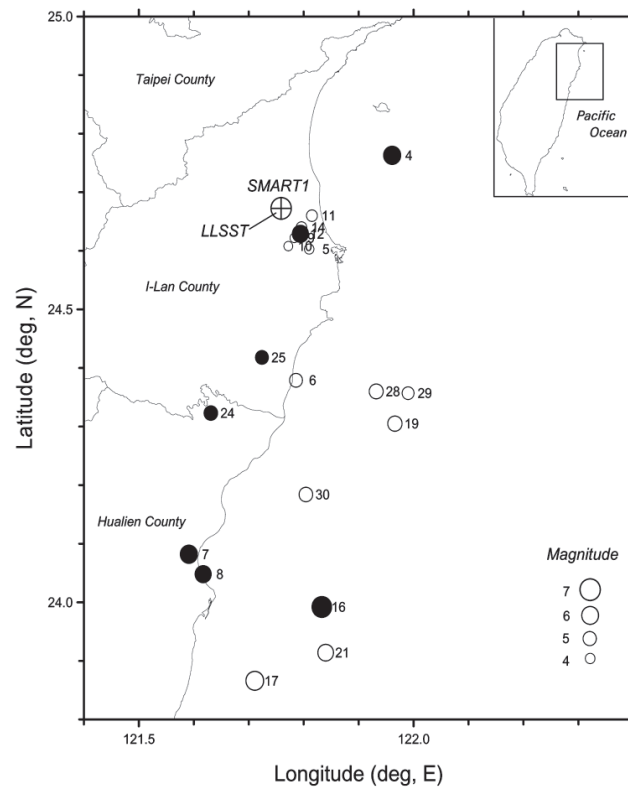


Fig. 3. Epicenter distribution of earthquakes analyzed in this study. Each number at the right side of the epicenter is the serial number in the exclusive seismic catalog for the LLSST array. The earthquakes, which have triggered recording systems both in the LLSST array and SMART1 array simultaneously, are denoted as solid circles for comparison purposes of ground strains.

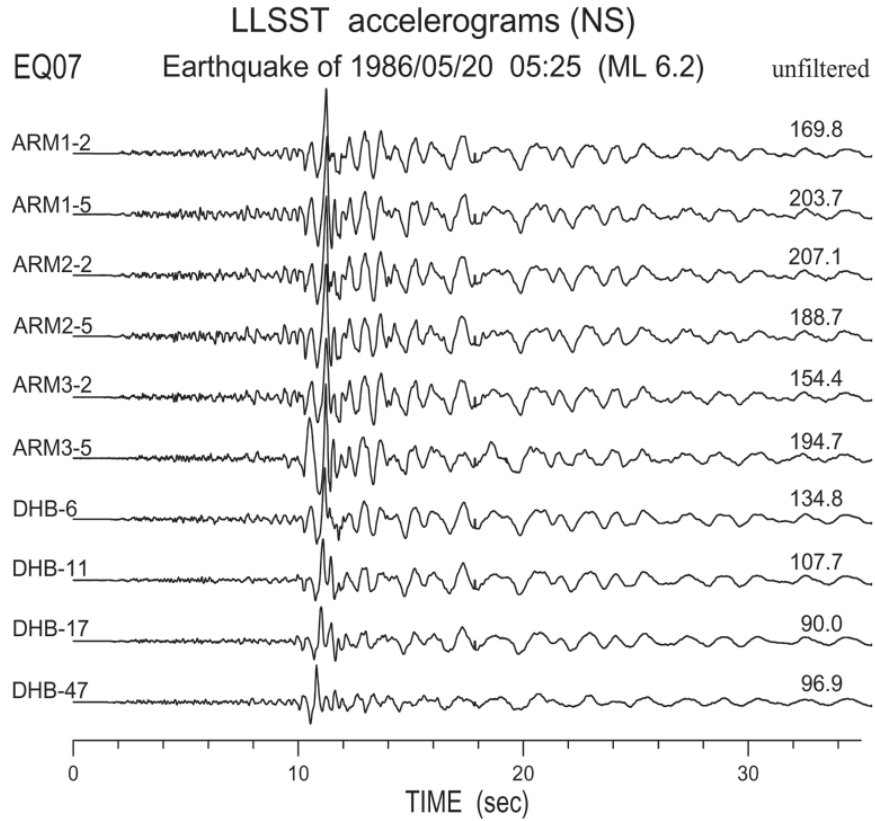


Fig. 4. Examples of accelerograms recorded by the LLSST array during the 20 May 1986 earthquake in Hualien. The number at the end of each seismogram is the peak ground acceleration in units of cm s^{-2} .

The displacement gradient can be characterized by a 3×3 matrix, whose elements can be reduced to six independent terms under the constraint that the vertical component of stress tensor is zero at the free surface (Spudich et al. 1995; Bodin et al. 1997). Each component of the strain tensor, therefore, may be derived from related displacement gradients by solving the equation:

$$\Delta u_i = (\partial u_i / \partial s_j) \Delta s_j \quad , \quad (1)$$

where $i, j = x, y, z$ refer to directions east, north, and up, respectively. Δu_i is the differential of recorded displacements. Δs_j represents the difference in spatial coordinates between two stations and can be replaced by Δx , Δy , and Δz , respectively. Dynamic strain is then estimated for each time step.

In practice, a least-squares procedure was used to obtain the average strain from more than two estimations from multiple station pairs among the array, the reason being that the average station spacing is still not small enough to satisfy the assumption of uniform incidence of plane waves under the array. A minor error in the displacement field produced by double-integration for accelerograms could also become a source of variance. Moreover, some abnormal displacement gradients, caused by dividing by a very small coordinate differential in the appointed orientation, must be discarded from the least-squares fittings.

5. ARRAY ANALYSES FOR DISPLACEMENT GRADIENT

The fifteen free-field stations of the LLSST array were deployed along three arms radiating outward from a central containment model for studying soil-structure interaction (Fig. 2). It is necessary to assess effects on the ground motion due to nearby man-made structures before estimating ground deformation in free field. Four subarrays, named here as: AR17, AR28, AR38, and AR90, were thus defined by stations included within triangular areas with vertices located at the second, third, fourth, and fifth stations along each arm, respectively. The apertures of these subarrays are 17, 28, 38, and 90 m, respectively, as implied in their names. As a result, a larger number of displacement gradient estimations would be used in the least-squares method for subarrays with larger aperture.

Acceleration recordings for the Hualien earthquake ($M_L = 6.2$) of 20 May 1986 were analyzed. Some of the waveforms are shown in Fig. 4. After the procedures previously described, six dynamic displacement gradients were calculated for the data of each subarray, approximated by the ratios: $\Delta u_y / \Delta y$, $\Delta u_y / \Delta x$, $\Delta u_x / \Delta y$, $\Delta u_x / \Delta x$, $\Delta u_z / \Delta y$, and $\Delta u_z / \Delta x$ (abbreviated by NN, NE, EN, EE, ZN, and ZE in the following figures of this article, respectively). Comparisons of those results are presented in Fig. 5 and, in general, large discrepancies between arrays are not evident except in the horizontal gradients of vertical motion. Larger distortions are consistently attributed to shear waves and surface waves in each component. It can be noticed that slight, higher frequency fluctuations in dynamic gradient, particularly for $\Delta u_y / \Delta y$ and $\Delta u_x / \Delta y$, occur just following direct S waves (AR17 array data). This phenomenon suggests the possibility of interference in the incident plane waves caused by scattering or reflections. The containment model may be a source of such a disturbance. In addition, peak horizontal gradients associated with the vertical displacement of shear wavetrains using AR17 data are about five times larger than those calculated from the recordings at other larger subarrays. The first and second station on each arm (i.e., the inner elements of AR17) are located within 5 m of the wall of the containment model, which has its base buried about 3 m below the ground. When incident waves propagate into the soil layers in a nearly vertical direction, a predictable disturbance of the wave field will occur accompanied by strong shaking similar to S waves, and it is perhaps more obvious in the vertical component due to reflection waves and scattered energy rebounding off the structure. This kind of effect generally results in larger estimation of ground strain. However, this influence can be reduced through least-squares matching by using a larger aperture subarray, even when the inner stations of AR17 are included.

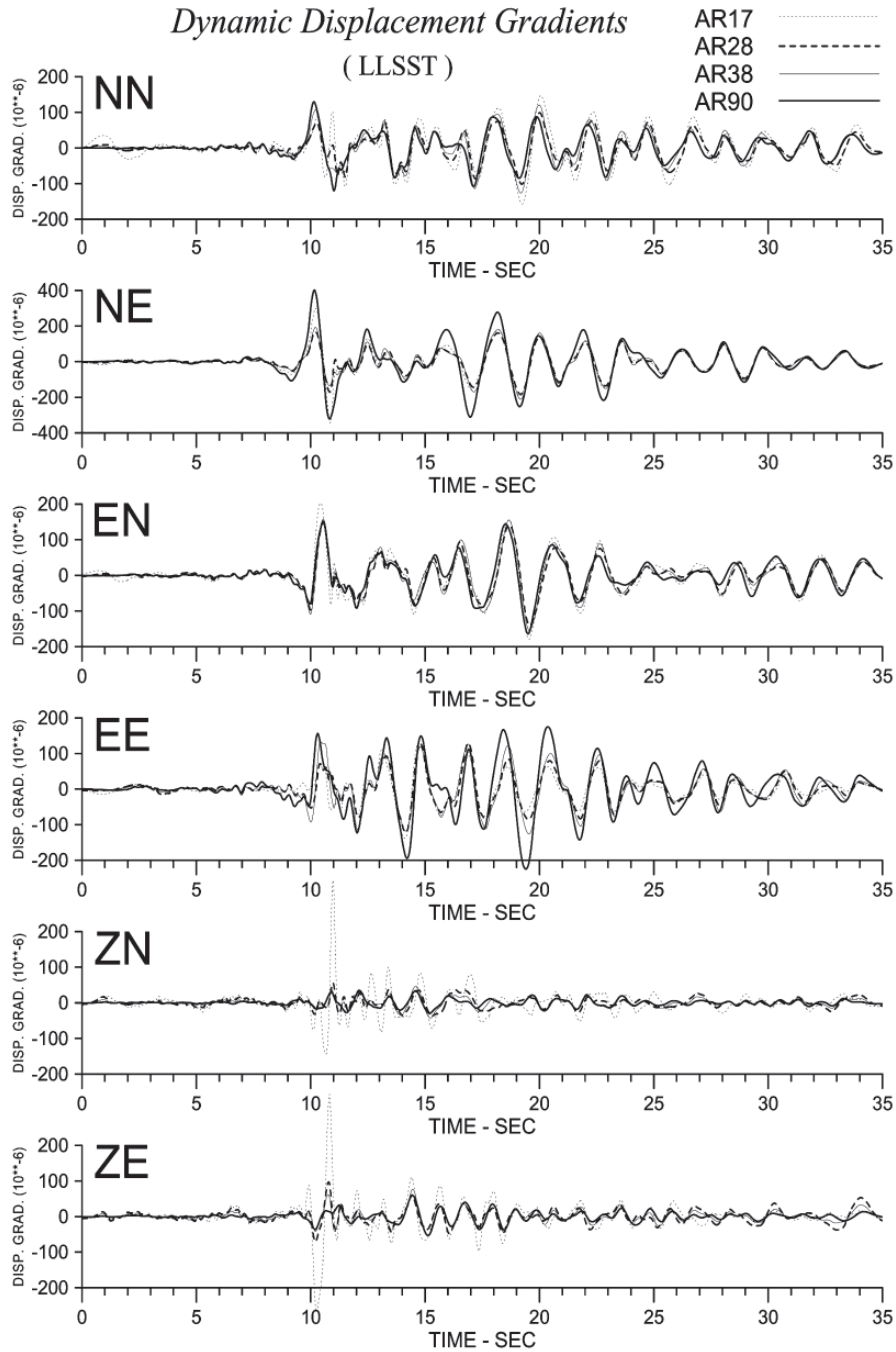


Fig. 5. Comparisons between dynamic displacement gradients respectively estimated from four subarrays with different aperture described in the text. The line type denotations are indicated at the upper right corner.

Is it better to assemble more data recorded from stations of the array to estimate the ground strains? To answer this question, a simple analysis was implemented in this study. For each subarray, all six dynamic displacement gradients were calculated using only three vertex station data and taking all recordings of stations enclosed within the defined triangular region, respectively. The comparisons of peak gradients for the cases are shown in Fig. 6. The results from subarray AR17 are obviously unreliable because of the aforementioned interference.

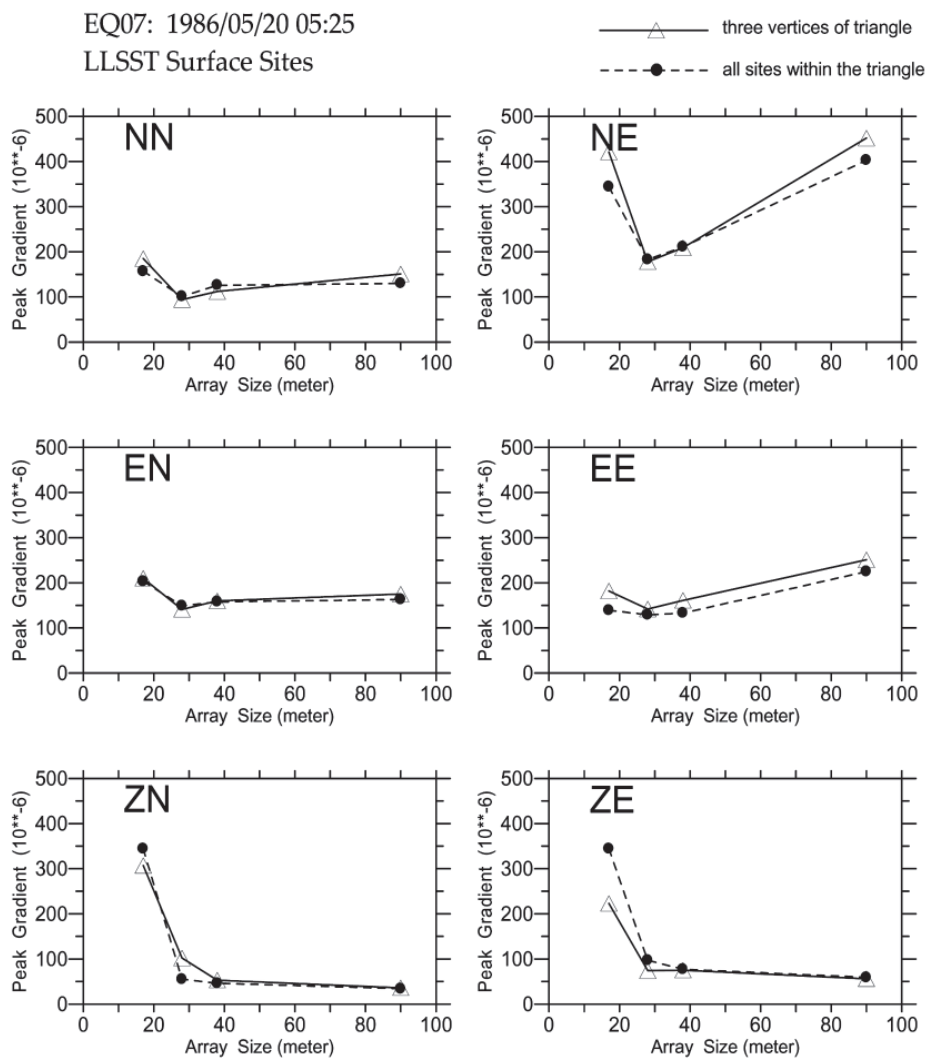


Fig. 6. Comparisons between maximum displacement gradients estimated from all enclosed stations (solid circles) and from only three vertex stations (open triangles), respectively, for the subarrays with different aperture.

However, the unusual peak gradients of $\Delta u_y / \Delta x$ derived from AR90 (i.e., all the surface stations of LLSST) have no explanation currently. Most estimates, revealed from larger subarrays AR28, AR38, and AR90, demonstrate only slight dependence on array aperture and imply the noise added to ground motion due to the containment model can be neglected beyond about 30 m. Moreover, the 3-station results are very close to those of all-station data with average differences of about 10%. The analyses conclude that good estimations of ground strain can be obtained using only three 3-component seismometers recording at stations configured in a regular triangle and these estimations are valid even for stations with maximum separation of about 100 m, which is similar to the dimension of other microarrays such as the Roma array of Mexico City (Bodin et al. 1997). Consideration of signal resolution and stability, using more of the available data excluding those of AR17 subarray, was then given for the following analyses.

6. DYNAMIC GROUND DEFORMATIONS FOR THE 20 MAY 1986 EARTHQUAKE

Figure 7 shows the estimated dynamic shear strain at the ground's surface of LLSST sites during the Hualien earthquake of 20 May 1986. This result was derived from recordings at all surface stations excluding those near the structure. The larger strains apparently are associated with shear and surface waves, similar to displacement gradients. In this case, peak shear strain of 210μ occurs with direct S-waves whilst 186μ of strain occurs in the group of surface waves dominated by a period of about 2.5 sec. Such levels of strains induced seismically have been observed to cause liquefaction (Dobry et al. 1981).

The LLSST array consists of two sets of borehole sensors, named DHA and DHB, at four different depths and in horizontal separation of about 47 m along the north-south arm (Fig. 2). During the 1986 Hualien earthquake, a complete set of borehole recordings provides an opportunity to understand the variation in vertical gradients of displacement below the ground. Like

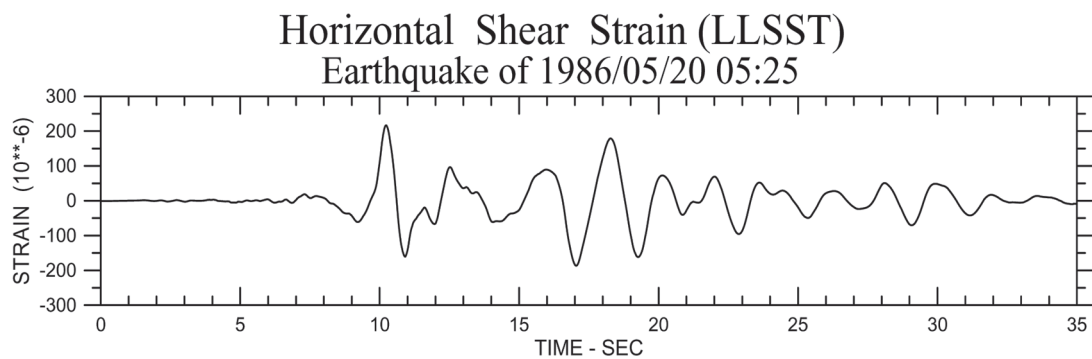


Fig. 7. Dynamic horizontal shear strain estimated at the surface of the LLSST array during the Hualien earthquake of 20 May 1986.

the array analysis for surface stations, a cross examination of displacement gradients in vertical profile was implemented by comparing results estimated from four combinations of stations as follows: (a) DHB-6 borehole station (6 m in depth) and the fifth station of ARM1, (b) DHB-6 and DHA-6 borehole stations and the second and fifth stations of ARM1, (c) DHB-6 and DHA-6 borehole stations and all stations along ARM1, and (d) DHB-6 and DHA-6 borehole stations and all surface stations of the LLSST. The comparisons reveal no obvious discrepancies in both amplitude and the dynamic form, as shown in Fig. 8, which relates to the gradient $\Delta u_y / \Delta z$ between the surface and a 6-m depth. The peak vertical gradient accompanied by shear waves is in the range of $1500 \sim 2000 \mu$, which is larger than those of horizontal differential motions by a factor of about 10.

For calculating each displacement gradient at a depth interval below the top 6 m, four stations of DHA- and DHB-borehole arrays at two boundary depths were used and, hence, an average can be obtained by four estimates from associated station pairs. By inspecting results shown in Fig. 9, the following characteristics can be described: (1) Predominant vertical gradients in all components take place with direct S-waves, which are greater than those of horizontal differential motions at the free surface. (2) The largest gradients are observed at a depth ranging from 6 to 11 m. (3) Peak gradients in vertical components are much smaller than those in horizontal components. (4) Gradients associated with surface waves are apparently identified but not as remarkable as those on the free surface when compared with results shown in Fig. 5.

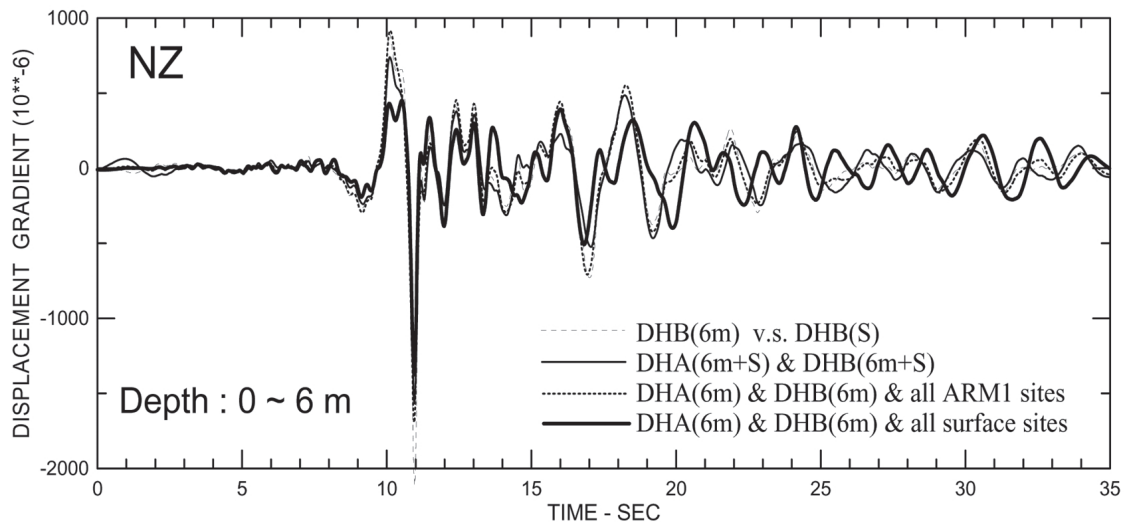


Fig. 8. Comparison among the dynamic vertical gradients of NS-component displacements ($\Delta u_y / \Delta z$) recorded at the ground surface and a depth of 6 m, during the Hualien earthquake of 20 May 1986, for different combinations of recordings. The character 'S' in parenthesis of the legend represents the nearest surface station to the related downhole array.

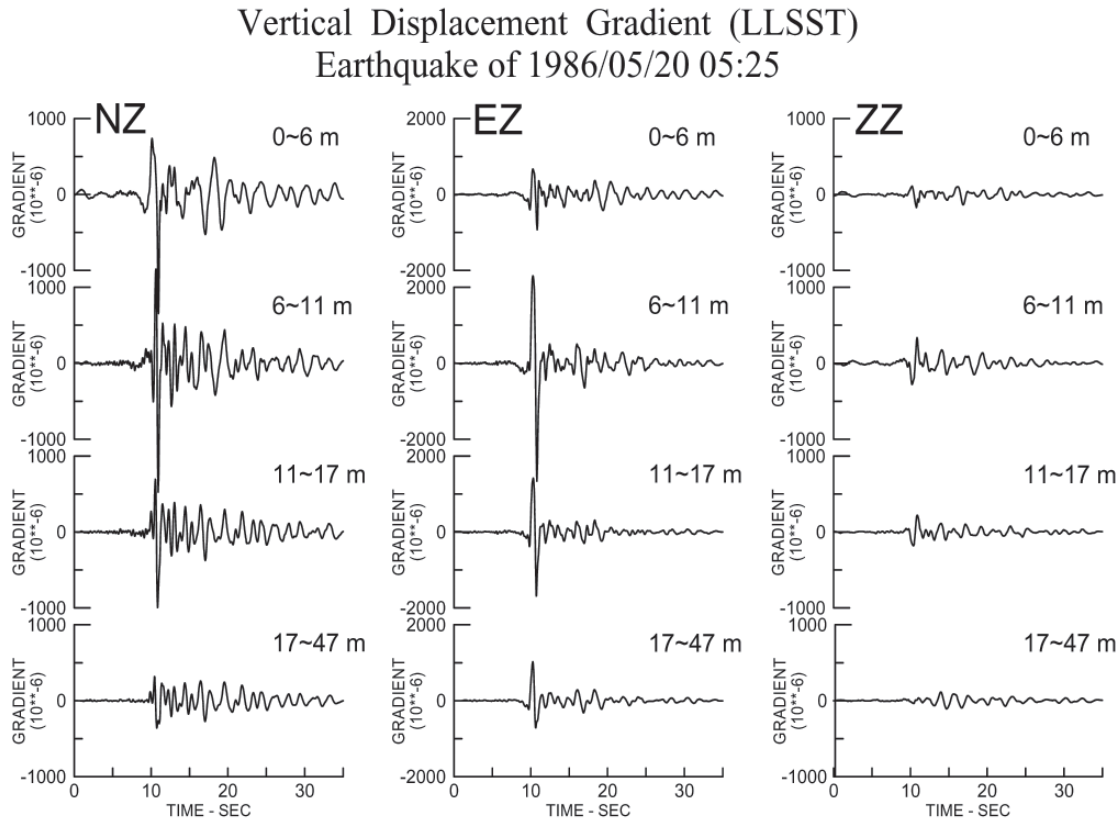


Fig. 9. Estimated dynamic vertical displacement gradients at different ranges of depth at the LLSST array site during the Hualien earthquake of 20 May 1986.

It is reasonable to expect such results because the phase delay between different depths will be larger than that of the same depth when incident waves propagate near vertically through the top sedimentary layer with a lower velocity. Bodin et al. (1997) also mentioned such phenomenon by examining the vertical distribution of gradients from receiver functions of surface waves in different modes. They suggested that displacements and related gradients depend not only on these functions but also on the excitation of the modes at the source, and on propagation effects between source and receiver. To understand the character of the deformation field under the ground in more detail, more data from different sources are necessary. Unfortunately, the dataset used here is the only complete one that includes recordings at every depth for both borehole arrays during the operation period of the LLSST array.

7. COMPARISONS WITH SINGLE-STATION ESTIMATIONS

In the absence of small aperture seismic-array data in the regions of interest, ground strain can be alternatively estimated using seismograms recorded at an individual station. In developing the single-station estimation, all derivations are based on the assumption that seismic energy travels as planar S-waves along a source-receiver great circle path in a laterally homogeneous or slowly-varying medium. Newmark (1967) suggested that the peak shear strain in soils is proportional to the horizontal ground velocity:

$$\varepsilon = v_{\max} / c \quad . \quad (2)$$

The factor c is the apparent phase velocity, which is proportional to shear wave velocity of the top layer and should theoretically depend on source depth and epicentral distance. This is only strictly true if the disturbance propagates as a plane wave within a homogeneous material. This simple relationship has been widely studied and permits possible applications in mapping deformation fields at given areas for seismic microzonation (Trifunac et al. 1996; Trifunac and Lee 1996; Todorovska and Trifunac 1996; Singh et al. 1997).

To examine the applicability of the single-station method at the LLSST site, peak horizontal ground strains computed from integrated displacement recordings of surface stations were compared with those estimated from equation (2) for the nineteen earthquakes (see Fig. 3 and Table 1). The purpose of these comparisons is to establish their relationship or, more precisely, a proportional expression. Based on the conclusions of our previous array analyses, only the two outermost available stations of each arm, composing an array with station spacing of about 30 ~ 90 m, were considered for getting more stable estimations in this study. The maximum horizontal strain, which can be supposed to be the “true” one, is picked out from the dynamic ground deformation derived using equation (1). In terms of the single-station method, the same stations in the array were used to estimate the apparent velocities of dominant S waves. The accelerograms were first integrated and simultaneously filtered with a frequency band of 0.3 ~ 3 Hz to produce velocity time histories. Utilizing a time window of width 4 sec totally enclosing the predominant shear waves, cross-correlation matching between any two tapered horizontal component waveforms was performed to obtain time shifts between two S phases and consequently, the apparent phase velocity from the station distance along the propagation direction reasonably assumed to be the azimuth of the source-receiver great circle. By eliminating abnormally high velocities due to poor resolution of the time shift between stations aligned in a direction almost perpendicular to the wave path, the averaged horizontal apparent velocities of S waves are shown in Fig. 10a for the analyzed earthquakes. Most results are in the range 2.4 ~ 4.0 km s⁻¹ with a 12% to 40% deviation. From the filtered velocity waveforms of surface stations excluding the innermost ones, the average maximum ground velocity can easily be derived by taking the geometric mean of PGVs in two horizontal components, and is shown in Fig. 10b. Therefore, peak ground horizontal strains are estimated by dividing the maximum ground velocity by apparent velocity along the surface. Figure 11 represents the comparisons between strains from these two approaches. It is obvious for most cases that both methods can provide close estimations in a range from several μ to about 10⁻⁴.

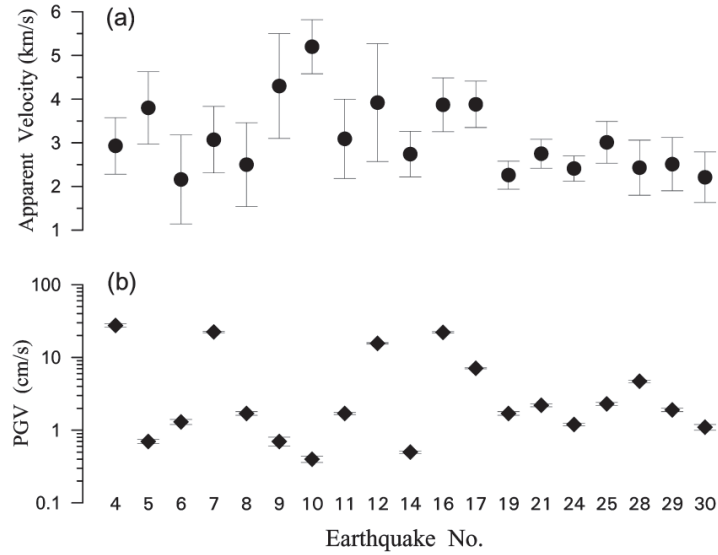


Fig. 10. (a) Averaged horizontal apparent velocities of S waves, and (b) geometric means of peak ground velocities of two horizontal components of analyzed earthquakes.

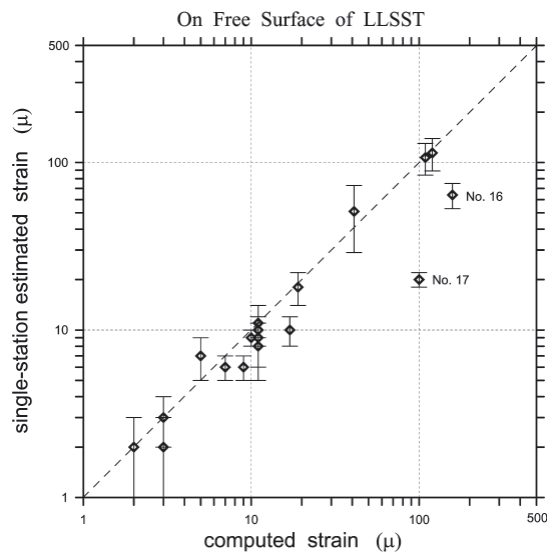


Fig. 11. Comparisons of horizontal peak ground strains estimated by the single-station method and those computed from the horizontal displacement gradients, using LLSST data. The vertical error bars indicate one standard deviation. The diagonal dashed line represents 1 : 1 proportionality.

Before judging the applicability of the single-station method, two largely under-estimated strains [earthquakes no.16 and no.17 of the LLSST catalog (Table 1)] must be investigated to determine the source of the discrepancies. Strains of 158 and 100 μ were estimated for earthquakes 16 and 17, respectively, using displacement gradients, while respective strains of 64 and 20 μ were given using the single-station method. These two moderate earthquakes, located about 80 km south of the array, have generated remarkable surface-wave energy propagating through the Lanyang plain. The dynamic horizontal displacement gradients and strains are dominated by the arrivals of surface waves lagging about 5 ~ 20 sec behind the S waves (Fig. 12).

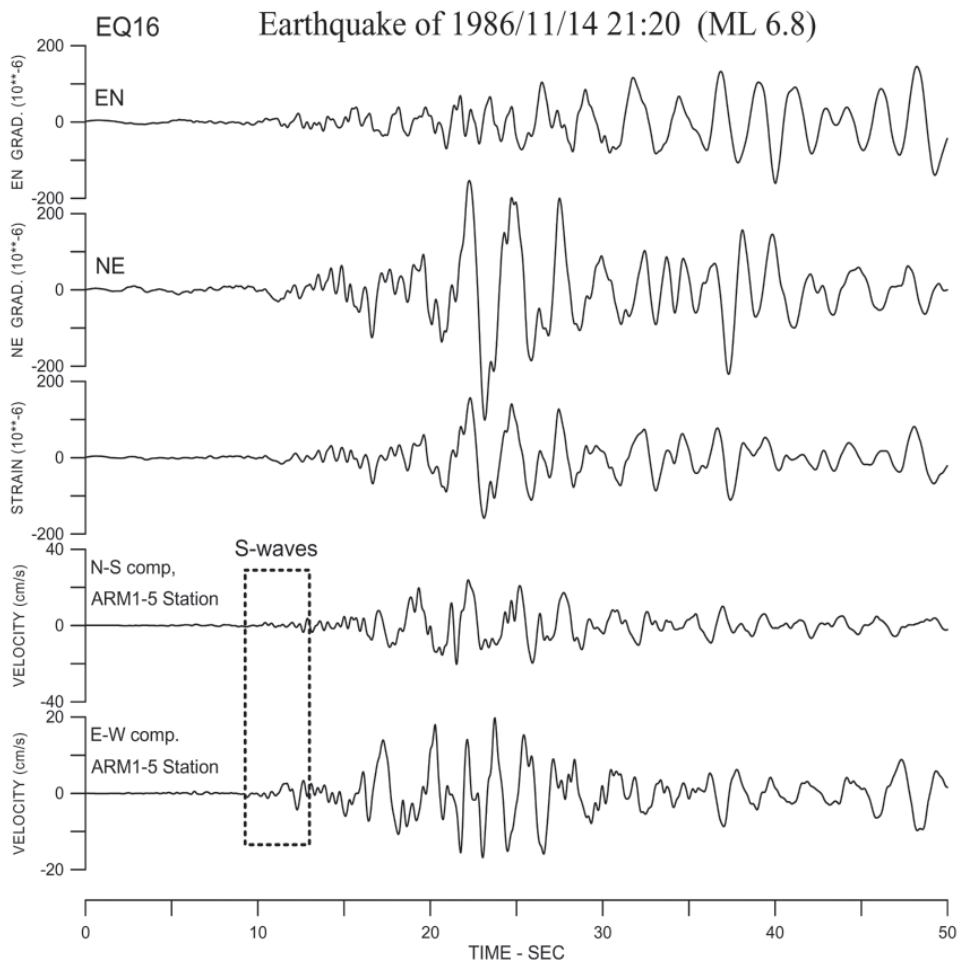


Fig. 12. Horizontal shear displacement gradients (upper two traces), dynamic shear ground strain (middle), and the integrated velocity histories of horizontal components (lower two traces) associated with the earthquake of 14 November 1986.

That is to say higher phase velocities ($\sim 3.87 \text{ km s}^{-1}$), associated with shear waves, induced under-estimations for peak strain. For a general interpretation of equation (2), peak ground velocity should correspond to the apparent velocity of the same phase, which can be difficult to identify. Therefore, an alternative way of moving cross-correlation matching over an entire waveform was tried in this study to obtain phase velocities for a sequence of waves. To do this, the width of the tapering window is basically 2 sec, but suitable adjustment is allowed when complex waveforms are analyzed. Here, each moving step of the tapering window is one half of the width. The variation in apparent velocity is then aligned with the horizontal component of velocity to allow searching for the target phases expected to accompany peak strain (see Fig. 13). Consequently, the peak strains of 80 and 53 μ were re-estimated by the method for the two earthquakes. Those are, therefore, closer to the results computed from displacement gradients.

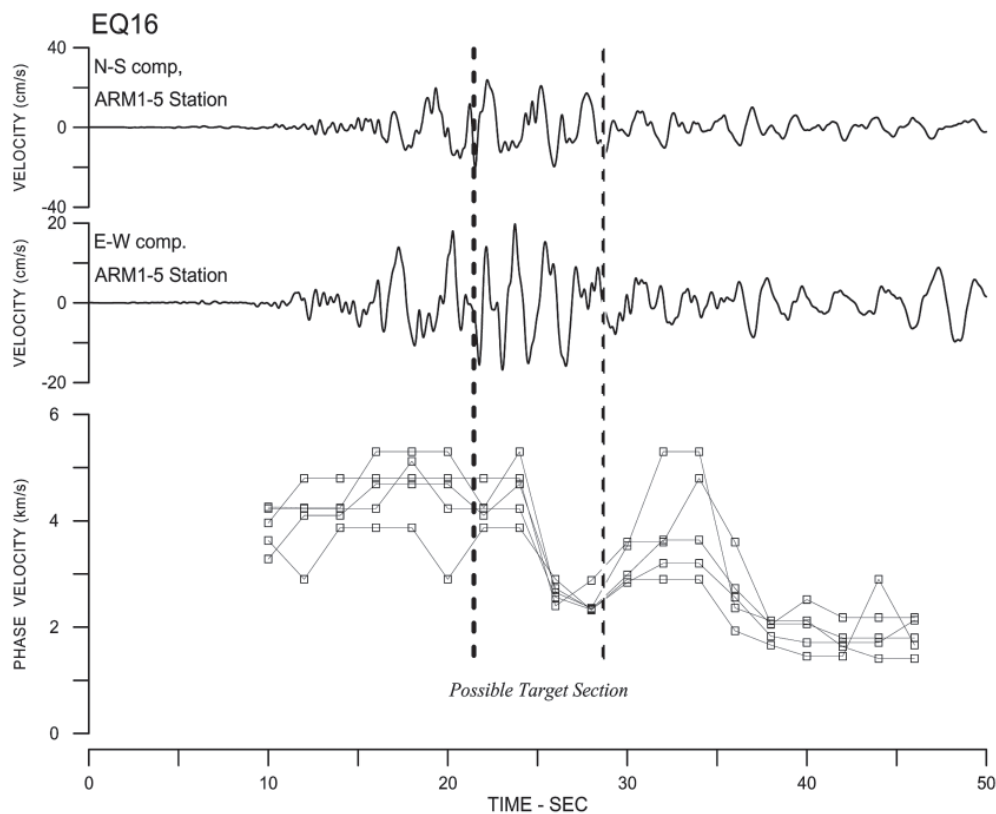


Fig. 13. Examples of horizontal velocity seismograms (upper two traces) and the phase velocities derived by a moving cross-correlation technique between different pairs of station recording. The section between the dashed lines has been judged as the possible target for peak strain to appear.

8. DISCUSSION AND CONCLUSIONS

Without seismograms recorded by a dense array, ground strains can be estimated using the single-station method as given by ground velocity and apparent propagation velocity along the ground surface. Based on the method's assumption, it is suggested that peak strain must be carefully determined by searching all phases in the time history, particularly when ground motion contains obvious surface-wave energy. From the comparative results shown in this study, the possibility exists for evaluating ground deformation fields in other metropolitan regions during large earthquakes. The estimations of peak horizontal strain at the LLSST site are in the range $1 \sim 150 \mu$ for the moderate earthquakes analyzed here. The logarithm of peak strain appears to be directly proportional to the magnitude of an earthquake as shown in Fig. 14. In addition, the relationship between ground strain and epicentral distance is not clear, which may be associated with the incident angle and consequentially apparent velocity of propagating waves. However, a level of strain over 100μ is of interest from an engineering viewpoint and, unfortunately, does not display an explicit proportional relationship due to a lack of observations.

To extend the strain-magnitude relationship for major earthquakes ($M > 7$), a proper strategy, given budget limitations, is to set up a few seismometers at the same site to await big

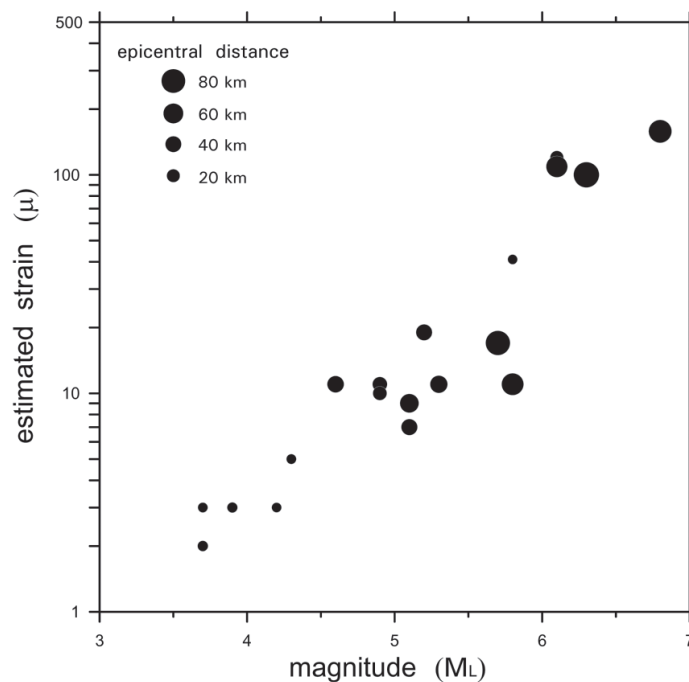


Fig. 14. Relationship of peak ground strain and local magnitude of earthquakes. The diameter of the solid circle is proportional to the epicentral distance as shown in the legend.

earthquakes. Meanwhile, about forty free-field accelerometers evenly deployed in the Lanyang plain underlain by a thick recent alluvium, operating under the Central Weather Bureau of Taiwan's TSMIP (Taiwan Strong Motion Instrumentation Program) network since 1993 (Shin 1993), have a chance of resolving this problem. The average station spacing is about 2 ~ 3 km, similar to those in other metropolitan areas such as the Taipei basin. For implementing a wide range investigation of horizontal peak ground strain, the single-station method seems to be the only way forward here, even though most accelerometers have been replaced by second-generation instruments equipped with precise GPS units for overcoming inconsistent timing.

Basically, getting "correct" apparent velocities along the ground surface with the propagating waves is a key factor. A simple test has been implemented in this study to verify the applicability of this method when applied to a case with large station spacing. The SMART1 array mainly occupied a circular area with a diameter of about 4 km in Lotung City (Fig. 1) and totally covered the LLSST array. Among the nineteen earthquakes analyzed herein, seven of those (marked in Table 1) were also well-recorded by the SMART1 array. For each earthquake, six SMART1 stations, always including station O08 nearby the LLSST array, were selected for analysis to simulate the station deployment of the regular strong-motion network on the same scale of station separation. By using the data processing previously described, especially the moving cross-correlation technique for obtaining dynamic phase velocities, peak strains were estimated by the single-station approach from SMART1 data and compared to the results from the LLSST data (Fig. 15). When taking strain from the LLSST data as a basis, results revealed discrepancies were not more than 50%. In general, this is not too bad.

It is well known that ground strains are site specific. The site conditions for most stations of the TSMIP network in the Lanyang plain have been categorized as class D or E based on the geologic and geomorphologic data (Lee et al. 2001). According to the available P-S logging profiles under the project established by the CWB and National Center for Research on Earthquake Engineering (NCREEE), the average shear wave velocities of strata in the upper 30 m at those stations in the central and eastern parts of the plain range from 190 to 260 m sec⁻¹. An average shear wave velocity of about 205 m sec⁻¹ for the top 35 m of soil layer at the LLSST site has been revealed from geological testing (Wu et al. 1987). In the SMART1 area, the soil layer has P-wave velocity of about 430 to 760 m sec⁻¹ with a thickness of about 18 m (Wen and Yeh 1984). Assuming a similar Poisson's ratio (~0.48) with that at the LLSST site, the shear wave velocity would be in the range 140 ~ 160 m sec⁻¹, which could certainly increase to approach the range described above if depths were extended from 18 to 30 m. If the property of the top soil layer is a significant factor in ground strains, similar shear wave velocity in the Lanyang plain, at least, implies that it is possible to investigate the ground deformation field over the entire plain during strong earthquakes using TSMIP network data and the method of this study.

In summary, the critical steps of this method include: (1) selecting strong-motion histories recorded at surface stations with a close spacing (< 3 km); (2) synchronizing their recording times and integrating them to velocity histories accompanied by proper filtering; (3) using the moving cross-correlation process to obtain apparent velocities of target phases; and (4) calculating peak strain using the relationships of the single-station method. Basically, the method-

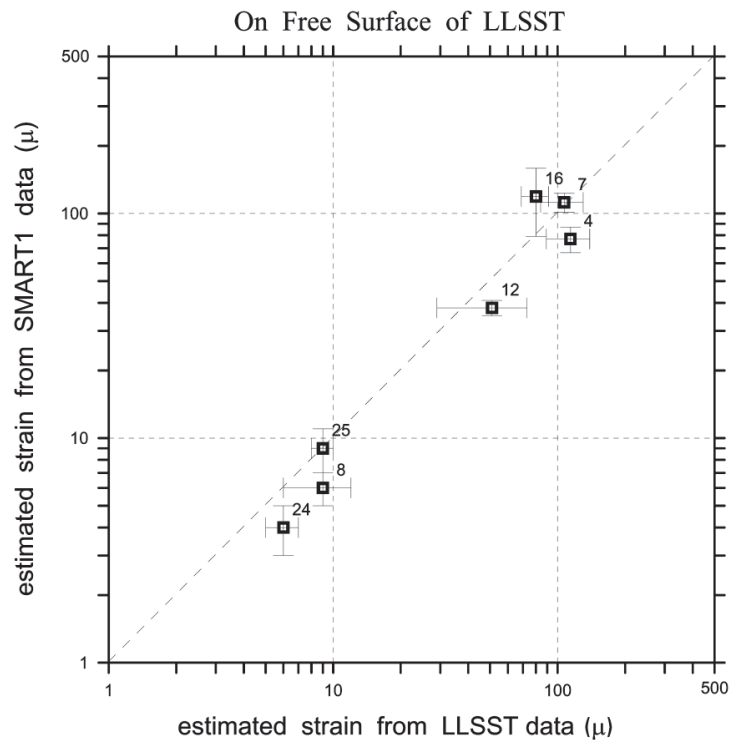


Fig. 15. Comparisons of horizontal peak ground strains estimated respectively from the LLSST and SMART1 data. The denoted numbers are the sequential numbers in the LLSST catalog in Table 1. Both the vertical and horizontal error bars indicate one standard deviation, respectively. The diagonal dashed line represents 1 : 1 proportionality.

ology for microzonation mapping of peak ground strain can easily be applied to most metropolitan areas in Taiwan, especially, e.g., the region along the Chelungpu fault which ruptured in 1999 Chi-Chi earthquake. By correlating strains to damage patterns, the results of such analyses can provide guidelines in the design of new and upgrading of existing long-span structures.

Acknowledgements The author would like to thank Dr. W. G. Huang for providing the LLSST and SMART1 data through the authority of the Institute of Earth Sciences, Academia Sinica, Taiwan, and also for much help in data preparation. The author is also thankful to Professors H. B. Havenith and M. D. Trifunac for their critical reviews and comments which helped to improve the manuscript. This research was supported by the Taiwan Earthquake Research Center (TEC) funded through the National Science Council, Republic of China (NSC) under Grant No. NSC92-2625-Z-231-003. The TEC contribution number for this article is 00012.

REFERENCES

- Anderson, J. G., P. Bodin, J. N. Brune, J. Prince, S. K. Singh, R. Quaas, and M. Onate, 1986: Strong ground motion from the Michoacan, Mexico, Earthquake. *Science*, **233**, 1043-1049.
- Bard, P. Y., and M. Bouchon, 1985: The two-dimensional resonance of sediment-filled valleys. *Bull. Seismol. Soc. Am.*, **75**, 519-541.
- Bodin, P., J. Gomberg, S. K. Singh, and M. Santoyo, 1997: Dynamic deformations of shallow sediments in the Valley of Mexico, Part I: Three-dimensional strains and rotations recorded on a seismic array. *Bull. Seismol. Soc. Am.*, **87**, 528-539.
- Bolt, B. A., Y. B. Tsai, K. Yeh, and M. K. Hsu, 1982: Earthquake strong motions recorded by a large near-source array of digital seismographs. *Earthq. Eng. Struc. Dyn.*, **10**, 561-573.
- Bonilla, M. G., 1991: The Marina District, San Francisco, California: Geology, history, and earthquake effects. *Bull. Seismol. Soc. Am.*, **81**, 1958-1979.
- Bouchon, M., 1980: The motion of the ground during an earthquake: Part 1: The case of a strike-slip fault. *J. Geophys. Res.*, **85**, 356-366.
- Bouchon, M., and K. Aki, 1982: Strain, tilt, and rotation associated with strong ground motion in the vicinity of earthquake faults. *Bull. Seismol. Soc. Am.*, **72**, 1717-1738.
- Chiang, S. C., 1976: A seismic refraction prospecting of the Ilan plain. *Mining Tech.*, **14**, 215-221.
- Dobry, R., K. H. Stokoe, R. S. Ladd, and T. L. Youd, 1981: Liquefaction susceptibility from S-wave velocity, in situ testing to evaluate liquefaction susceptibility. Proc. ASCE Natl. Convention.
- Frankel, A., 1994: Dense array recordings in the San Bernardino Valley of Landers-Big Bear aftershocks: Basin surface waves, Moho reflections, and three-dimensional simulations. *Bull. Seismol. Soc. Am.*, **84**, 613-624.
- Gomberg, J., and P. Bodin, 1994: Triggering of the $M_s = 5.4$ Little Skull Mountain, Nevada, earthquake with dynamic strains. *Bull. Seismol. Soc. Am.*, **84**, 844-853.
- Gomberg, J., and D. Agnew, 1996: The accuracy of seismic estimates of dynamic strains: An evaluation using strainmeter and seismometer data from Pinon Flat Observatory, California. *Bull. Seismol. Soc. Am.*, **86**, 212-220.
- Hanks, T. C., and A. G. Brady, 1991: The Loma Prieta earthquake, ground motion, and damage in Oakland, Treasure Island, and San Francisco. *Bull. Seismol. Soc. Am.*, **81**, 2019-2047.
- Lee, C. T., C. T. Cheng, C. W. Liao, and Y. B. Tsai, 2001: Site classification of Taiwan free-field strong-motion program. *Bull. Seismol. Soc. Am.*, **91**, 1283-1297.
- Lee, V. W., 1990: Surface strains associated with strong earthquake shaking. *Proc. JSCE*, **422**, 187-194.
- Moczo, P., P. Labak, J. Kristek, and F. Hron, 1996: Amplification and differential motion due to an antiplane 2D resonance in the sediment valleys embedded in a layer over the half-space. *Bull. Seismol. Soc. Am.*, **86**, 1434-1446.
- Newmark, N., 1967: Problems in wave propagation in soil and rock, Proc. Inter. Symp. On

- Wave Propagation & Dynamic Properties of Earthquake Materials, Albuquerque, 7-26.
- Saito, M., 1968: Synthesis of rotational and dilatational seismograms. *J. Phys. Earth*, **16**, 53-62.
- Shin, T. C., 1993: Taiwan strong motion instrumentation program, Sym. Taiwan Strong Motion Instrumentation Program, Taipei, 1-10.
- Singh, S. K., M. Santoyo, P. Bodin, and J. Gomberg, 1997: Dynamic deformations of shallow sediments in the Valley of Mexico, Part II: Single-station estimates. *Bull. Seismol. Soc. Am.*, **87**, 540-550.
- Smith, S. W., J. E. Ehrenberg, and E. N. Hernandez, 1982: Analysis of the El Centro differential array for the 1979 Imperial Valley earthquake. *Bull. Seismol. Soc. Am.*, **72**, 237-258.
- Spudich, P., L. K. Steck, M. Hellweg, J. B. Fletcher, and L. M. Baker, 1995: Transient stresses at Parkfield, California, produced by the M 7.4 Landers earthquake of June 28, 1992: Observations from the UPSAR dense seismograph array. *J. Geophys. Res.*, **100**, 675-690.
- Teng, T. L., and J. Qu, 1996: Long-period ground motions and dynamic strain field of Los Angeles basin during large earthquakes. *Bull. Seismol. Soc. Am.*, **86**, 1417-1433.
- Todorovska, M. I., and M. D. Trifunac, 1996: Hazard mapping of normalized peak strain in soils during earthquakes: Microzonation of a metropolitan area. *Soil Dyn. Earthq. Eng.*, **15**, 321-329.
- Trifunac, M. D., M. I. Todorovska, and S. S. Ivanovic, 1996: Peak velocities and peak surface strains during Northridge, California, earthquake of 17 January 1994. *Soil Dyn. Earthq. Eng.*, **15**, 301-310.
- Trifunac, M. D., and V. W. Lee, 1996: Peak surface strains during strong earthquake motion. *Soil Dyn. Earthq. Eng.*, **15**, 311-319.
- Wen, K. L., and Y. T. Yeh, 1984: Subsurface structure under the SMART1 array. *Bull. Inst. Earth Sci. Acad. Sin.*, **4**, 51-72.
- Wu, W. T., S. L. Foo, C. C. Chiang, and L. Y. Cheng, 1987: Final testing reports of foundation soils for Lotung nuclear power plant model, Report of Taiwan Power Company.
-
- Chung, J. K., 2007: Estimation of ground strain using accelerograms recorded by two dense seismic arrays at Lotung, Taiwan. *Terr. Atmos. Ocean. Sci.*, **18**, 715-737, doi: 10.3319/TAO.2007.18.4.715(T).